4. Kukkonen AK, Pelkonen AS, Mäkinen-Kiljunen S, Voutilainen H, Mäkelä MJ. Ara h 2 and Ara 6 are the best predictors of severe peanut allergy: a double-blind placebo-controlled study. Allergy 2015;11:1239-45.
5. Nozawa A, Okamoto Y, Movérare R, Borres MP, Kurihara K. Monitoring Ara h 1, 2 and 3-sIgE and sIgG4 antibodies in peanut allergic children receiving oral rush immunotherapy. Pediatr Allergy Immunol 2014;25:323-8.
6. Vickery BP, Scurlock AM, Kulis M, Steele PH, Kamilaris J, Berglund JP, et al. Sustained unresponsiveness to peanut in subjects who have completed peanut oral immunotherapy. J Allergy Clin Immunol 2014;133:468-75.
7. Krause S, Reese G, Randow S, Zennaro D, Quaratino D, Palazzo P, et al. Lipid transfer protein (Ara h 9) as a new peanut allergen relevant for a Mediterranean allergic population. J Allergy Clin Immunol 2009;124:771-8.e5.
8. Glaumann S, Nilsson C, Asarnoj A, Movérare R, Johansson SG, Borres MP, et al. IgG4 antibodies and peanut challenge outcome in children IgE-sensitized to peanut. Pediatr Allergy Immunol 2015;26:386-9.
9. Santos AF, James LK, Bahnson HT, Shamji MH, Couto-Francisco NC, Islam S, et al. IgG4 inhibits peanut-induced basophil and mast cell activation in peanut-tolerant children sensitized to peanut major allergens. J Allergy Clin Immunol 2015;135:1249-56.

Available online December 1, 2016.
http://dx.doi.org/10.1016/j.jaci.2016.09.054

Tofacitinib relieves symptoms of stimulator of interferon genes (STING)–associated vasculopathy with onset in infancy caused by 2 *de novo* variants in *TMEM173*

To the Editor:

Stimulator of interferon genes (STING), which is encoded by transmembrane protein 173 *(TMEM173)*, is an important mediator in initiating innate immune responses by detecting aberrant DNA species or cyclic di-GMP-AMP (cGAMP) in the cytosol and driving synthesis of type I interferon.[1-3] cGAMP molecules, which are produced by cyclic GMP-AMP synthase, bind to STING homodimers embedded in the endoplasmic reticulum membrane and eventually cause phosphorylation of interferon regulatory factor 3 by activating Tank-binding kinase 1 (TBK1). Patients with activating mutations of STING display early onset of chronic inflammation and vasculopathy caused by increased type I interferon signaling, a condition termed STING-associated vasculopathy with onset in infancy (SAVI).[2,3] Improved understanding of STING's function and its implications in disease pathogenesis has suggested new potential avenues of disease treatment options through modulating STING signaling pathway components.

A 9-year-old Korean boy presented with systemic hyperinflammatory symptoms, including skin lesions, brain infarctions, and pulmonary dysfunction. From 6 months of age, he experienced recurrent infections, including acute otitis media, pneumonia, and gastroenteritis. Telangiectatic skin mottling on both the hands and feet was evident from 12 months of age, which progressed to the extremities and face over time (Fig 1, *A*, and see Fig E1 in this article's Online Repository at www.jacionline.org). At 5 years of age, he was hospitalized because of pneumococcal meningitis, and brain magnetic resonance imaging and magnetic resonance angiography revealed evidence of infarction in the right parietal area. Chest computed tomography at 8 years of age showed evidence of obliterative bronchiolitis with peribronchial inflammation (Fig 1, *B*). Consequently, the patient experienced sudden left leg weakness and headache. Brain magnetic resonance imaging revealed acute infarction in the right anterior watershed area and subarachnoid hemorrhages, and magnetic resonance angiography showed diffuse advanced luminal irregularities throughout the cerebral arteries (Fig 1, *C*). At 9 years of age, a low nasal bridge was apparent and likely caused by a perforated nasal septum (Fig 1, *D*). Generalized telangiectatic rashes on the cheeks, nose, arms, legs, hands, and feet, with gangrenous lesions, were associated with his recurrent infections. He had slight dyspnea, which worsened on physical exertion but needed continuous supplemental oxygen of 1 L/min or more to maintain an oxygen saturation measured by pulse oximetry of between 90% and 95%. Wheezing and crackles were audible in both lower lung fields.

Trio-based whole-exome sequencing was performed (Fig 1, *E*, and see Table E1 in this article's Online Repository at www.jacionline.org) to search for variants that were specifically found in the patient. Among the candidates, 2 *de novo* variants of *TMEM173* appeared to be the most promising based on known disease associations with the patient's phenotype (Fig 1, *F*, and see Table E2 and Figs E2 and E3 in this article's Online Repository at www.jacionline.org). To determine whether the 2 variants occurred in the same chromosome (in *cis*) or on different chromosomes (in *trans*), we amplified a 3.8-kb fragment of *TMEM173* that encompasses both variants, sequenced it using the PacBio sequencing platform, and found that both variants occurred in the paternal chromosome (see Fig E2).

The variants were not observed in any of the public (1000 Genomes and ExAC) or private (1060 healthy Koreans) databases, and the corresponding amino acid residues are strongly conserved among vertebrate orthologs (Fig 1, *G*). The changes were predicted to be damaging by using variant effect prediction software, and the amino acids are located on the transmembrane (p.Ser102Pro) and cytoplasmic domains (p.Phe279Leu), which are involved in homodimerization and are distant from previously reported pathogenic mutations on exon 5 (Fig 1, *H*, and see Tables E2 and E3 in this article's Online Repository at www.jacionline.org). Analysis of the protein structure reveals that Phe279 is located on the N-terminus of the fourth α-helix, which converges physically with the N-terminus of the first α-helix, possibly affecting nearby amino acids, including Asn154 and Val155, which were found to be mutated in patients with SAVI (Fig 1, *I*). Analysis of Ser102 was unavailable, although a recent study suggests that Ser103 is important for maintaining proper subcellular localization.[4]

Based on the known functions of STING, we investigated further the functional consequences of the STING variants. First, patient-derived fibroblasts displayed increased expression of IFN-β, helping to explain the increased inflammatory responses in the patient (Fig 2, *A*). To understand the molecular basis for increased IFN-β expression, we monitored IFN-β promoter activity by expressing the various mutant STING proteins in HEK293T cells (Fig 2, *B*). As the cGAMP concentration increases, cells expressing the mutant STING proteins had increased IFN-β promoter activity compared with cells expressing the wild-type STING but with 2 notable differences from previous observations. First, the double-mutant STING (S102P + F279L) showed stronger activity than the STING with a single mutation (S102P or F279L), implying an additive mode of action by the 2 variants. Second, at a baseline level, the mutant STING proteins barely displayed any IFN-β promoter

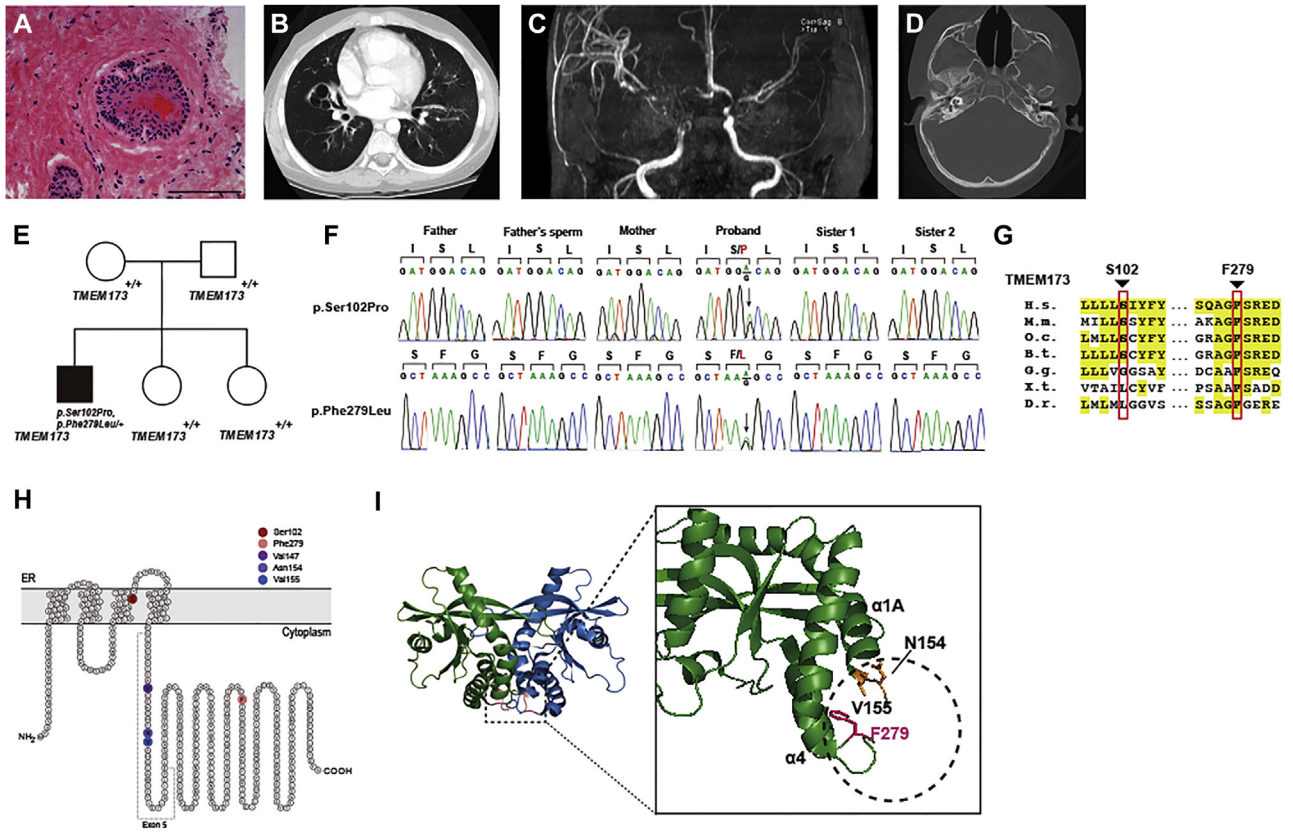

FIG 1. Two patient-specific variants in *TMEM173* are associated with SAVI. The phenotypes associated with SAVI are shown. **A,** Histologic analysis of a skin biopsy sample stained with hematoxylin and eosin. *Bar* = 100 μm. **B,** Chest computed tomographic scan taken at 8 years of age. **C,** Brain magnetic resonance angiography. **D,** Computed tomography of the head showing perforated nasal septum. **E,** Pedigree of the patient's family. The proband has 2 *de novo TMEM173* variants in the paternal chromosome. **F,** Sanger sequence traces confirming the 2 variants. **G,** Evolutionary conservation of the *TMEM173* Ser102 and Phe279 residues in orthologs from selected vertebrate species. **H,** Primary structure of *TMEM173*, depicting trans–endoplasmic reticulum membrane and cytoplasmic domains. Variant sites of the patient are shown in red (Ser102) and orange (Phe279); previously reported variants in patients with SAVI are shown in purple (Val147), navy (Asn154), and blue (Val155). The known variants clustered together in a small region of the cytoplasm domain (exon 5). **I,** Three-dimensional model of the TMEM173 homodimer complex *(left)* with a magnified view of the domains where Phe279 on α-helix 4 and known variants (Asn154 and Val155) on α-helix 1A physically converge *(right). B.t., Bos Taurus*; *D.r., Danio rerio*; *G.g., Gallus gallus*; *H.s., Homo sapiens*; *M.m., Mus musculus*; *O.c., Oryctolagus cuniculus*; *X.t., Xenopus tropicalis*.

activity, whereas the V147L mutation showed increased activity even without cGAMP (Fig 2, *B* and *C*). This observation reflects the patient's delayed onset of disease at 6 months of age, whereas patients with the p.Val147Leu variant presented with infantile onset (see Table E3). Also, the patient is heterozygous for the p.Arg71His-p.Gly230Ala-p.Arg293Gln (HAQ) allele, which is known to confer an approximately 5-fold reduction in IFN-β promoter activity when unstimulated, partially explaining the patient's low basal promoter activity (see Fig E2).[5] Subsequent immunoprecipitation analyses revealed that the degree of homodimerization of STING was not altered in the presence or absence of cGAMP (Fig 2, *D*), but the 2 variants cooperatively conferred increased binding with the downstream factor TBK1, which was slightly increased by the individual mutation alone (Fig 2, *E*).

Previous analyses of patients with SAVI revealed decreased $CD4^+$ T-cell populations and normal $CD14^+$ monocyte levels within the population of PBMCs,[3] whereas our patient had slightly decreased $CD4^+$ T-cell and increased $CD14^+$ monocyte populations. Furthermore, phosphorylated STAT1 (p-STAT1) expression increased dramatically in patients' monocytes (Fig 2, *F* and *G*), demonstrating a distinct immunologic response compared with previous patients.[2,3] It has been reported that monocytes from patients with rheumatoid arthritis and systemic lupus erythematosus are more sensitive to IFN-γ signaling for STAT1 phosphorylation than monocytes from healthy donors.[6] Our patient displayed enhanced IFN-γ–secreting $CD4^+$ T-cell and serum IFN-γ levels (see Fig E4 in this article's Online Repository at www.jacionline.org), which were also different from the previously reported patients with SAVI.[3] Thus IFN-γ signaling sensitization in monocytes from our patient possibly contributed to the increased p-STAT1 level in monocytes. The distinct immunologic alterations might be partially contributed by a different genetic background.[3] No agent directly targets

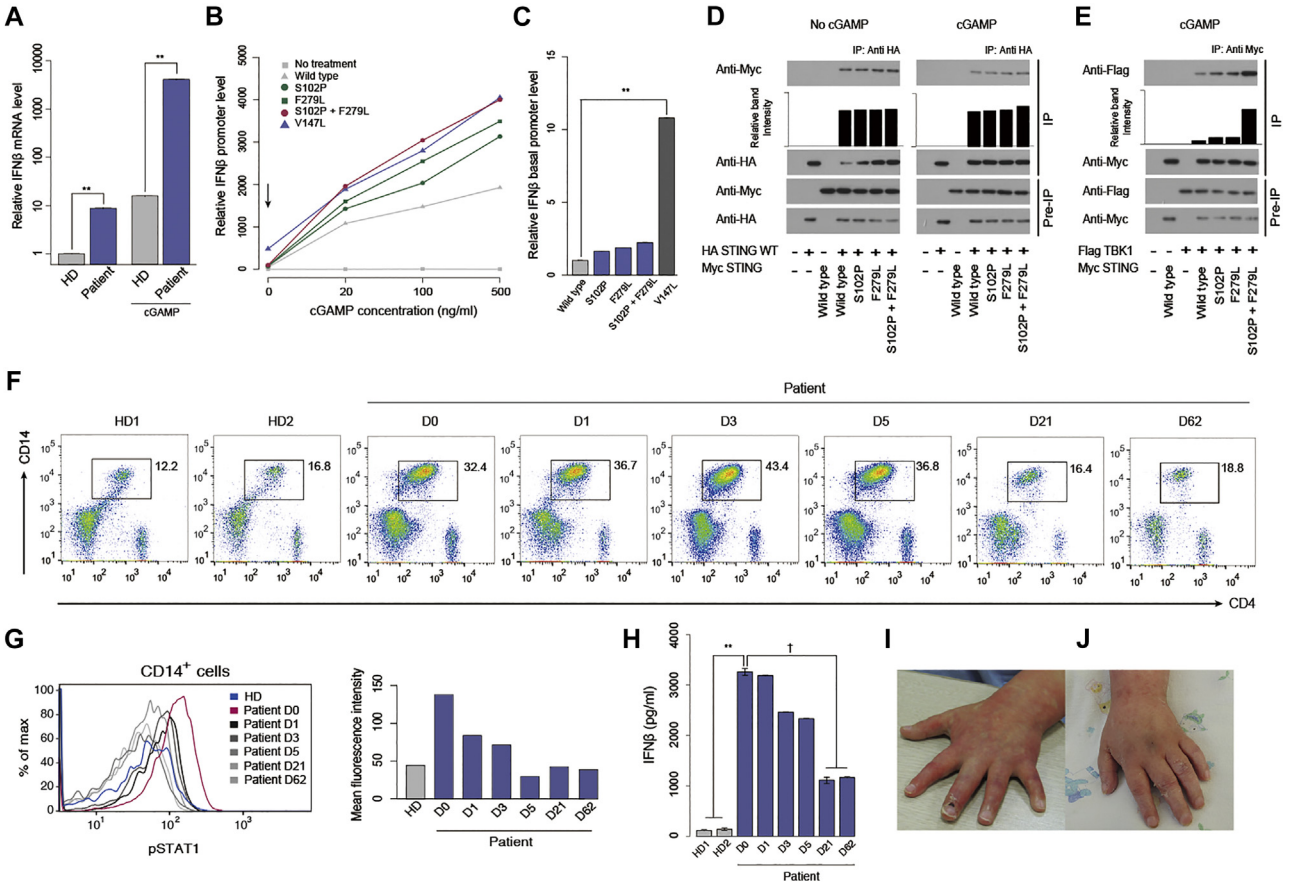

FIG 2. Tofacitinib reduces IFN-β signaling and improves skin lesions. **A,** Relative *IFNB* mRNA levels in primary cultured fibroblasts before and after stimulation with 2′3′-cGAMP (100 ng/mL). $^{**}P < .01$, Student *t* test. **B,** Levels of relative IFN-β promoter activity in wild-type, p.Ser102Pro (S102P), p.Phe279Leu (F279L), p.Ser102Pro, p.Phe279Leu double (S102P + F279L), and p.Val147Met (V147M) clone-transfected HEK293T cells after stimulation with cGAMP. **C,** Basal IFN-β promoter activity without cGAMP. $^{**}P < .01$, Student *t* test. **D,** STING homodimerization was examined by mixing and immunoprecipitating Myc-tagged STING monomers with various mutations and HA-tagged wild-type monomers expressed in HEK293T cells. **E,** Immunoprecipitation between various STING mutants and TBK1 in HEK293T cells. **F,** Flow cytometric analysis using the patient's and healthy donors' PBMCs. Days denotes the time in days after tofacitinib treatment. Numbers indicate the percentage of $CD4^{Int}CD14^{+}$ monocytes in PBMCs that were gated on forward scatter/side scatter scattergrams. **G** and **H,** p-STAT1 levels of $CD14^{+}$ cells (Fig 2, *G*) and the amount of serum IFN-β measured from the patient *(purple bars)* and healthy donors (*gray bars*; Fig 2, *H*). $^{**}P < .01$, Student *t* test. †$P < .01$, 1-way ANOVA. **I** and **J,** Improvement in hand skin lesions 62 days after tofacitinib treatment (Fig 2, *J*) compared with just before treatment (Fig 2, *I*).

STING, but tofacitinib controls the interferon signaling pathway by inhibiting Janus kinases and therefore is used in a number of disease models.[3,7] After treating the patient with tofacitinib (5 mg/d Xeljanz; Pfizer, New York, NY), the level of p-STAT1 in monocytes decreased rapidly and the monocyte population increased gradually to levels seen in healthy donors by the 21st day (Fig 2, *F* and *G*). In addition, the initial ratio of $CD4^{+}$ to $CD8^{+}$ cells in lymphocytes (0.61) was lower than that of healthy donors (1.12), and tofacitinib treatment further decreased this ratio (0.39 at day 1), but eventually, the ratio became comparable with that of healthy donors by the 62nd day (1.08; see Fig E5 in this article's Online Repository at www.jacionline.org). Also, inflammatory cytokine levels decreased rapidly (Fig 2, *H*, and see Figs E4-E6 in this article's Online Repository at www.jacionline.org). Three months of tofacitinib treatment improved the patient's telangiectatic skin lesions (Fig 2, *I* and *J*). However, the patient's pulmonary defect remained unchanged, perhaps because his bronchial damage persisted during the critical period of lung growth.

Here we report a patient with SAVI caused by 2 genetic changes in *STING* successfully treated with the Janus kinase inhibitor tofacitinib, which improved the patient's skin lesions. Recent studies have revealed the genetic mechanisms underlying Mendelian forms of autoimmune disorders caused by monogenic defects.[8] For example, we characterized and treated a patient with cytotoxic T lymphocyte–associated protein 4 haploinsufficiency with autoimmune infiltration with the cytotoxic T lymphocyte–associated protein 4 mimetic abatacept

to augment protein function and demonstrated improved clinical signatures.[9] As the genetic causes underlying idiopathic autoimmune diseases are uncovered more efficiently by using genome sequencing, more successful cases of drug repositioning to readily alleviate disease symptoms will become more commonplace.

We thank the patient and his family for their willing and active participation during the study.

Jieun Seo, BS[a]*
Jung-Ah Kang, MS[b]*
Dong In Suh, MD[c]*
Eun-Byeol Park, BS[d]
Cho-Rong Lee, MS[b]
Sun Ah Choi, MD[c]
Soo Yeon Kim, MD[c]
Yeji Kim, BS[e]
Sang-Heon Park, MS[b]
Michael Ye, PhD[f]
Soon-Hak Kwon, MD[g]
June Dong Park, MD, PhD[c]
Byung Chan Lim, MD[c]
Dong Hun Lee, MD, PhD[e]
Suk-Jo Kang, PhD[d]
Murim Choi, PhD[a,c]
Sung-Gyoo Park, PhD[b]
Jong-Hee Chae, MD, PhD[c]

From [a]Department of Biomedical Sciences, Seoul National University College of Medicine, Seoul, Korea; [b]Cell Logistics Research Center and School of Life Sciences, Gwangju Institute of Science and Technology, Gwangju, Korea; [c]Department of Pediatrics, Seoul National University College of Medicine, Seoul, Korea; [d]Department of Biological Sciences, Korea Advanced Institute of Science and Technology, Daejeon, Korea; [e]Department of Dermatology, Seoul National University College of Medicine, Seoul, Korea; [f]School of Liberal Arts and Sciences, Gwangju Institute of Science and Technology, Gwangju, Korea; [g]Department of Pediatrics, Kyungpook National University School of Medicine, Daegu, Korea. E-mail: murimchoi@snu.ac.kr. Or: sgpark@gist.ac.kr. Or: chaeped1@snu.ac.kr.

*These authors contributed equally to this work.

A portion of this study was supported by grants from the Korea Healthcare Technology R&D Project through the Korea Health Industry Development Institute (KHIDI), funded by the Ministry for Health and Welfare, Republic of Korea (HI12C0066; to J.-H.C.), and the Brain Research Program through the National Research Foundation of Korea (NRF) funded by the Ministry of Science, ICT and Future Planning (NRF-2014M3C7A1046049; to J.-H.C.). Also supported by grants from National Research Foundation of Korea (NRF-2016R1A5A1007318 and 2016M3C7A1905475); the Silver Health Bio Research Center of Gwangju Institute of Science and Technology (to S.-G.P.); and the Post-Genome Program of the National Research Foundation funded by the Ministry of Science, ICT & Future Planning (NRF-2014M3C9A2064686; to M.C.).

Disclosure of potential conflict of interest: E.-B. Park and S.-J. Kang receive grant support from National Research Foundation of Korea (Korean Ministry of Science, ICT, and future planning). The rest of the authors declare that they have no relevant conflicts of interest.

REFERENCES

1. Barber GN. STING: infection, inflammation and cancer. Nat Rev Immunol 2015;15:760-70.
2. Jeremiah N, Neven B, Gentili M, Callebaut I, Maschalidi S, Stolzenberg MC, et al. Inherited STING-activating mutation underlies a familial inflammatory syndrome with lupus-like manifestations. J Clin Invest 2014;124:5516-20.
3. Liu Y, Jesus AA, Marrero B, Yang D, Ramsey SE, Montealegre Sanchez GA, et al. Activated STING in a vascular and pulmonary syndrome. N Engl J Med 2014;371:507-18.
4. Surpris G, Chan J, Thompson M, Ilyukha V, Liu BC, Atianand M, et al. Cutting edge: novel Tmem173 allele reveals importance of STING N terminus in trafficking and type I IFN production. J Immunol 2016;196:547-52.
5. Yi G, Brendel VP, Shu C, Li P, Palanathan S, Cheng Kao C. Single nucleotide polymorphisms of human STING can affect innate immune response to cyclic dinucleotides. PLoS One 2013;8:e77846.
6. Karonitsch T, von Dalwigk K, Steiner CW, Bluml S, Steiner G, Kiener HP, et al. Interferon signals and monocytic sensitization of the interferon-gamma signaling pathway in the peripheral blood of patients with rheumatoid arthritis. Arthritis Rheum 2012;64:400-8.
7. Boyle DL, Soma K, Hodge J, Kavanaugh A, Mandel D, Mease P, et al. The JAK inhibitor tofacitinib suppresses synovial JAK1-STAT signalling in rheumatoid arthritis. Ann Rheum Dis 2015;74:1311-6.
8. Melki I, Crow YJ. Novel monogenic diseases causing human autoimmunity. Curr Opin Immunol 2015;37:1-5.
9. Lee S, Moon JS, Lee CR, Kim HE, Baek SM, Hwang S, et al. Abatacept alleviates severe autoimmune symptoms in a patient carrying a de novo variant in CTLA-4. J Allergy Clin Immunol 2016;137:327-30.

Available online December 29, 2016.
http://dx.doi.org/10.1016/j.jaci.2016.10.030

Effect of probiotics in prevention of atopic dermatitis is dependent on the intrinsic microbiota at early infancy

To the Editor:

Atopic dermatitis (AD) represents an allergic inflammatory disease, and is often the first disease present in a series of allergic diseases.[E1] There has been a dramatic increase in the prevalence of AD, with a tripling rate over the last 30 to 40 years in developed countries.[E2] Changes in environmental factors represent a likely driver.[E3] Bacterial exposure has been suggested as a key factor in atopic diseases, potentially through intestinal colonization and immunomodulation.[E4] Several trials have evaluated the role of probiotics in the prevention of atopic diseases and atopic sensitization, and there is compelling evidence for the effect on AD in early life.[1-3] Our mechanistic understanding of the effect, however, is still limited.

In line with the current conception, we have recently reported a 40% reduction in AD among 2-year-old children with maternal probiotic supplementation from the Prevention of Allergy among Children in Trondheim (ProPACT) cohort,[4] which is a randomized double- blind placebo-controlled study. Despite the major effect on AD, there was little or no effect of the probiotic on the gut microbiota composition through the first 2 years of life.[5,6] Therefore, it is unlikely that the AD effect is through gut microbiota modulation. A hypothesis that has not yet been explored, however, is that there are intrinsic differences in the gut microbiota that impact the effect of probiotics on AD.

The aim of the current work was to test the intrinsic microbiota hypothesis through reanalysis of the ProPACT 16S rRNA gene gut microbiota data set. We did this through analyses of 4 separate groups: probiotic intervention and AD (PA), probiotic intervention and no AD (PN), no probiotic intervention and AD (NA), and no probiotic intervention and no AD (NN).

We present results showing that the children developing AD not prevented by probiotic intervention (PA) have a divergent microbiota with an overrepresentation of *Bifidobacterium dentium* as compared with children from the other categories. The implications of these findings are that the intrinsic microbiota can have an association with the probiotic intervention effect.

ProPACT, a randomized double-blind intervention study, was started in 2003 and is described in detail in Dotterud et al.[4] In short, women received daily doses of probiotic-containing fermented milk starting from 36th gestation week until 3 months after birth.

METHODS

Subject

Written informed consent was obtained from the patient and his family for this study. All samples were collected for research purposes after approval by the Institutional Review Board of Seoul National University Children's Hospital (H-1406-081-588).

Whole-exome sequencing and variant calling

To understand the genetic basis of the clinical manifestations, we performed whole-exome sequencing (WES) of the patient and his parents. Preparation of genomic DNA, whole-exome capture with the NimbleGen V4 array, sequencing by using the Illumina HiSeq, read alignment, variant calling and filtering, and *de novo* variant calling procedures were described previously.[E1,E2] Raw sequence reads were generated by Theragen Etex Co, Ltd (Suwon, Korea). All the called variants were filtered according to the predicted effect on the protein and population frequencies (Table E2).

PCR and sanger sequencing

PCR amplification of 2 *de novo* variants was performed by using standard methods with specific primers (Table E4). The PCR condition included 1 cycle of predenaturation at 95°C for 2 minutes, 35 cycles of denaturation at 95°C for 20 seconds, annealing at 57°C for 40 seconds, elongation at 72°C for 40 seconds, and 1 cycle of postelongation at 72°C for 5 minutes. The products of PCR amplification were purified and sequenced by using the Sanger DNA sequencing method.

Orthologs

Full-length orthologous protein sequences among the vertebrates were identified by means of a BLAST search of human *TMEM173*, and sequences were extracted from GenBank. Orthologs were confirmed based on BLAST searches of the protein sequence against the human protein sequence, with the requirement that human *TMEM173* be the top hit and that protein sequences were aligned with the ClustalW algorithm.[E3] GenBank accession numbers for *TMEM173* included NP_938023.1 *(Homo sapiens)*, NP_082537.1 *(Mus musculus)*, XP_002710295.1 *(Oryctolagus cuniculus)*, NP_001039822.1 *(Bos taurus)*, XP_001232171.2 *(Gallus gallus)*, NP_001106445.2 *(Xenopus tropicalis)*, and NP_001265766.1 *(Danio rerio)*.

Protein structural analysis

STING secondary structures were identified by means of a UniProt search of human *TMEM173* and visualized proteoforms and annotated variants by using Protter (http://wlab.ethz.ch/protter/start/). STING C-terminal Domain 3D structure was extracted from the RCSB database (no. 4F5D) and analyzed by using PyMOL (https://www.pymol.org/).

Fibroblast activation and interferon mRNA quantification

Isolated fibroblasts from skin tissue of the patient or a healthy donor were stimulated with 100 ng/mL cGAMP for 24 hours, and the *IFNB* mRNA expression level was analyzed by means of quantitative RT-PCR analysis with specific primers (Table E4).

IFN-β promoter activity reporter assay

HEK293T cells, which are known to be devoid of STING,[E4] were transfected with pIFNβ-luc[E5] and pRenilla (Promega, Madison, Wis), and the STING expression vectors were cloned out from Jurkat cells. This *STING* clone does not carry the HAQ allele.[E6] Twenty-four hours after the transfection, cells were treated with the indicated concentration of cGAMP. After 24 hours, cells were lysed in 1× passive lysis buffer, and cellular debris was removed by means of centrifugation at 14,000 rpm for 5 minutes at 4°C. Firefly luciferase and Renilla luciferase activities were measured with 20 μL of lysate from each sample. The "fold stimulation" was calculated for each sample by dividing the luciferase activity in the sample normalized to Renilla luciferase activity by the activity of the sample containing empty expression vector.

Coimmunoprecipitation and immunoblot analysis

STING expression vector was constructed by inserting the *STING* open reading frame into the pcDNA3 expression vector. A QuickChange II XL site-directed mutagenesis kit (Agilent Technologies, Santa Clara, Calif) was used to mutate pcDNA3-Myc-STING to generate pcDNA3-Myc-STING (S102P), pcDNA3-Myc-STING (F279L), pcDNA3-Myc-STING (S102P/F279L), and pcDNA3pCMV-Myc-STING (V147L). For binding analysis between the various STING constructs, HEK293T cells were transfected with pcDNA3-HA-STING and pcDNA3-Myc-STING and immunoprecipitated with anti–hemagglutinin (HA) antibody. Then immunoprecipitated proteins were analyzed by means of immune blot analysis with anti-HA or anti-Myc antibodies. For binding analysis between STING and TBK1, HEK293T cells were transfected with pcDNA3-Myc-STING and pcDNA3-FLAG-TBK1 and immunoprecipitated with anti-HA antibody; immunoprecipitated proteins were subsequently analyzed by means of immune blot analysis with anti-Myc or anti-FLAG antibodies.

Serum cytokine analysis

Serum cytokines, including IL-17, IFN-γ, TNF-α, IL-10, IL-6, IL-4, and IL-2, in the patient's or healthy donors' serum were measured with the Cytokine Bead Array (BD Biosciences, San Jose, Calif) by using Canto II flow cytometer (BD Biosciences). Serum IFN-β levels were analyzed by means of ELISA (eBioscience, San Diego, Calif), according to the manufacturer's instructions.

PBMC population analysis (flow cytometry)

PBMCs were isolated from the patient's peripheral venous blood, collected with a Hickman catheter, and purified by means of density gradient centrifugation with Ficoll-Paque PLUS (GE Healthcare Life Sciences, Pittsburgh, Pa). Isolated cells were stained with the indicated fluorochrome-conjugated antibodies and analyzed with the LSR II flow cytometer (BD Biosciences). For intracellular staining, permeabilization solution (eBioscience) was used. The collected data were analyzed with FlowJo software (FlowJo, Ashland, Ore). Peridinin-chlorophyll-protein complex (PerCP)–cy5.5–conjugated anti-human CD3, allophycocyanin-conjugated anti-human CD19, Alexa Fluor 488–conjugated anti-human CD4, PerCP-cy5.5–conjugated anti-human CD8, allophycocyanin-eFluor 780–conjugated anti-human CD14, phycoerythrin-conjugated phosphor specific anti-human STAT1, Percp-cy5.5-conjugated anti-human IFN-γ, and phycoerythrin-conjugated anti-human IL-4 antibodies were purchased from eBioscience.

REFERENCES

E1. Choi M, Scholl UI, Ji W, Liu T, Tikhonova IR, Zumbo P, et al. Genetic diagnosis by whole exome capture and massively parallel DNA sequencing. Proc Natl Acad Sci U S A 2009;106:19096-101.

E2. Seo J, Choi IH, Lee JS, Yoo Y, Kim NK, Choi M, et al. Rare cases of congenital arthrogryposis multiplex caused by novel recurrent CHRNG mutations. J Hum Genet 2015;60:213-5.

E3. Sievers F, Wilm A, Dineen D, Gibson TJ, Karplus K, Li W, et al. Fast, scalable generation of high-quality protein multiple sequence alignments using Clustal Omega. Mol Syst Biol 2011;7:539.

E4. Burdette DL, Monroe KM, Sotelo-Troha K, Iwig JS, Eckert B, Hyodo M, et al. STING is a direct innate immune sensor of cyclic di-GMP. Nature 2011;478:515-8.

E5. Fitzgerald KA, McWhirter SM, Faia KL, Rowe DC, Latz E, Golenbock DT, et al. IKKepsilon and TBK1 are essential components of the IRF3 signaling pathway. Nat Immunol 2003;4:491-6.

E6. Yi G, Brendel VP, Shu C, Li P, Palanathan S, Cheng Kao C. Single nucleotide polymorphisms of human STING can affect innate immune response to cyclic dinucleotides. PLoS One 2013;8:e77846.

E7. Liu Y, Jesus AA, Marrero B, Yang D, Ramsey SE, Montealegre Sanchez GA, et al. Activated STING in a vascular and pulmonary syndrome. N Engl J Med 2014;371:507-18.

E8. Jeremiah N, Neven B, Gentili M, Callebaut I, Maschalidi S, Stolzenberg MC, et al. Inherited STING-activating mutation underlies a familial inflammatory syndrome with lupus-like manifestations. J Clin Invest 2014; 124:5516-20.

E9. Munoz J, Rodiere M, Jeremiah N, Rieux-Laucat F, Oojageer A, Rice GI, et al. Stimulator of interferon genes-associated vasculopathy with onset in infancy: a mimic of childhood granulomatosis with polyangiitis. JAMA Dermatol 2015;151:872-7.

E10. Chia J, Eroglu FK, Ozen S, Orhan D, Montealegre-Sanchez G, de Jesus AA, et al. Failure to thrive, interstitial lung disease, and progressive digital necrosis with onset in infancy. J Am Acad Dermatol 2016;74:186-9.

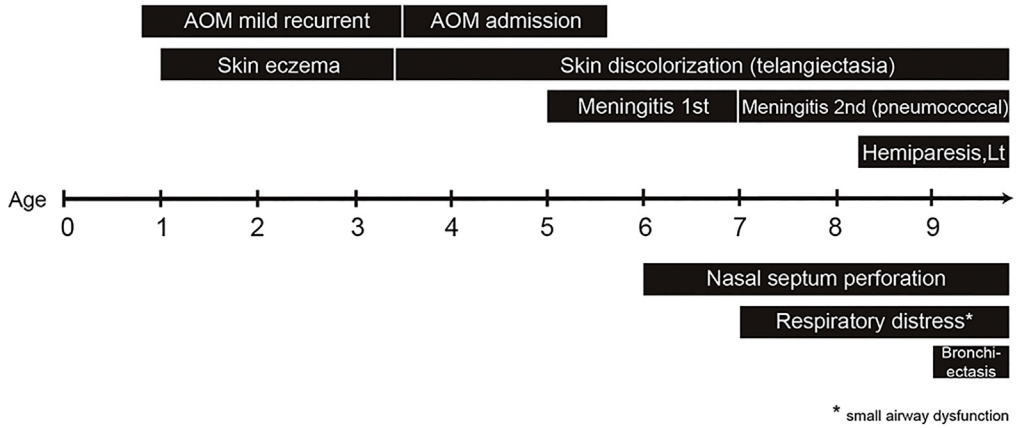

FIG E1. Clinical history of the patient. *AOM*, Acute otitis media.

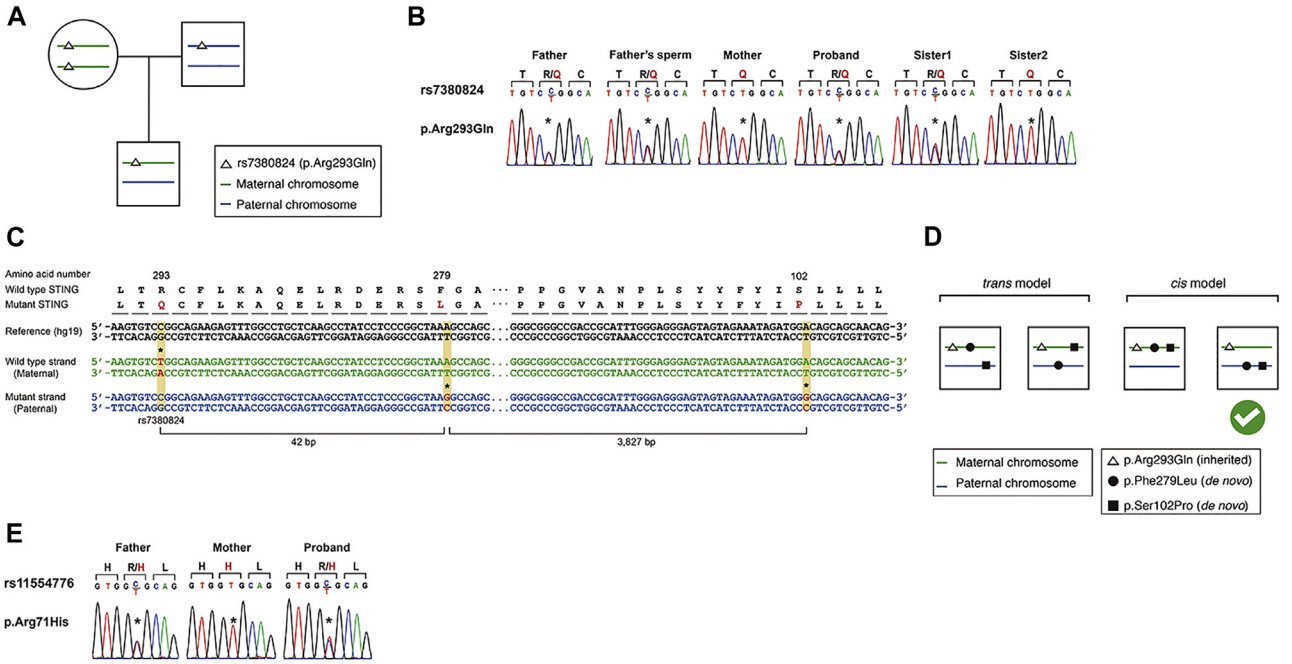

FIG E2. Long read sequencing result confirming the 2 *cis de novo* variants in *TMEM173*. **A,** The proband has a heterozygous common single nucleotide polymorphism (rs7380824; East Asian frequency 0.4205 from ExAC) inherited from the mother. **B,** Sanger sequence traces confirming the rs7380824 inheritance in the family. **C,** PacBio SMRT sequencing result of a 3.8-kb fragment from *TMEM173*, including rs7380824 and 2 *de novo* variants. **D,** Both *de novo TMEM173* variants occurred in the paternal chromosome (in *cis*). **E,** Genotype of rs11554776 (p.Arg71His). The variant positions are represented by the *asterisks*.

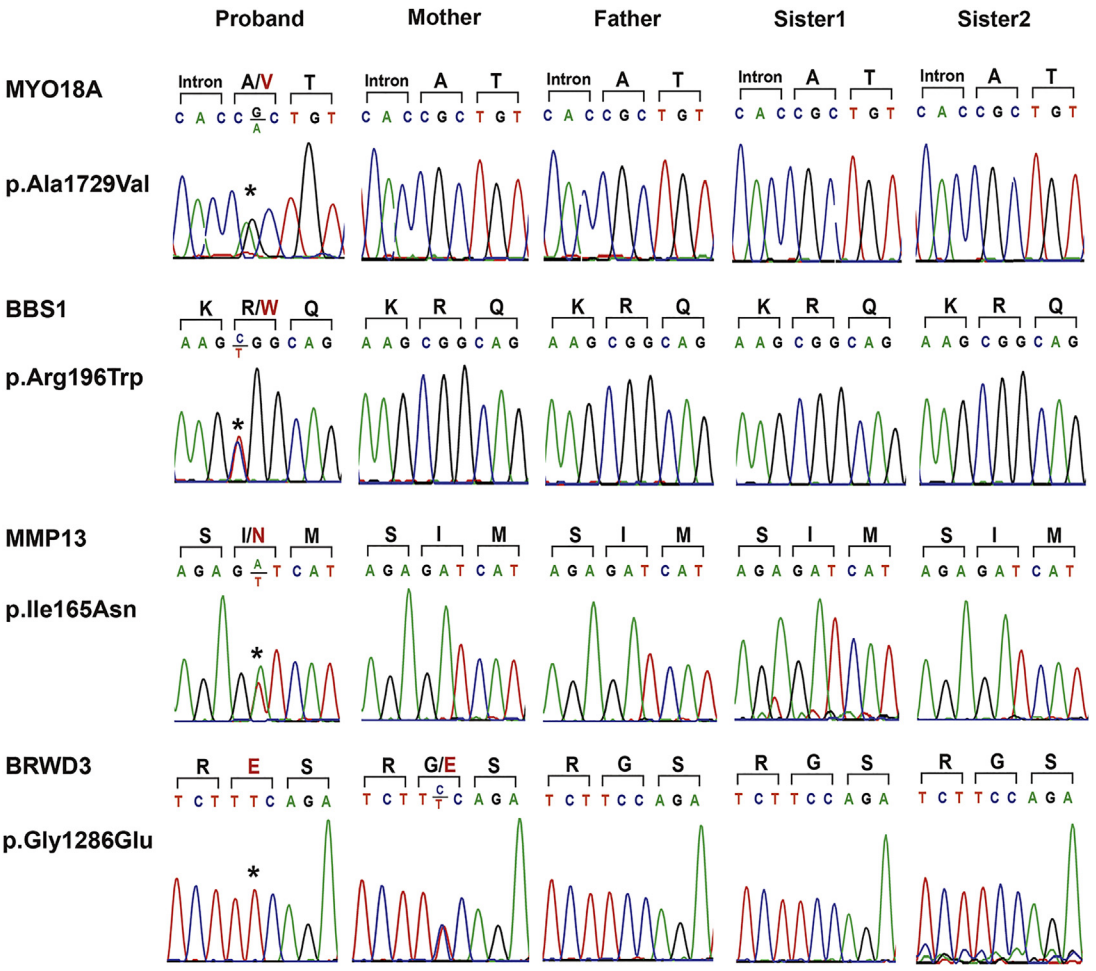

FIG E3. Sanger sequence traces confirming other variants from Table E1. The variant positions are represented by the *asterisks*.

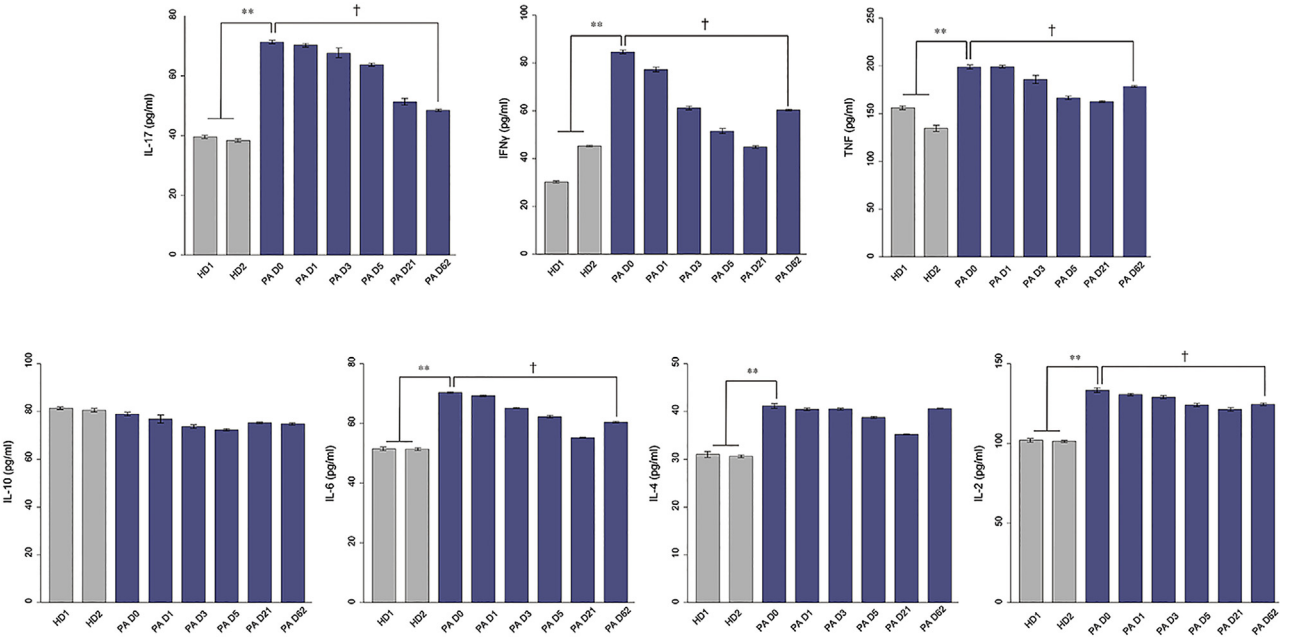

FIG E4. Cytokine levels from the patient's serum. $^{**}P < .01$, Student *t* test. †$P < .01$, 1-way ANOVA.

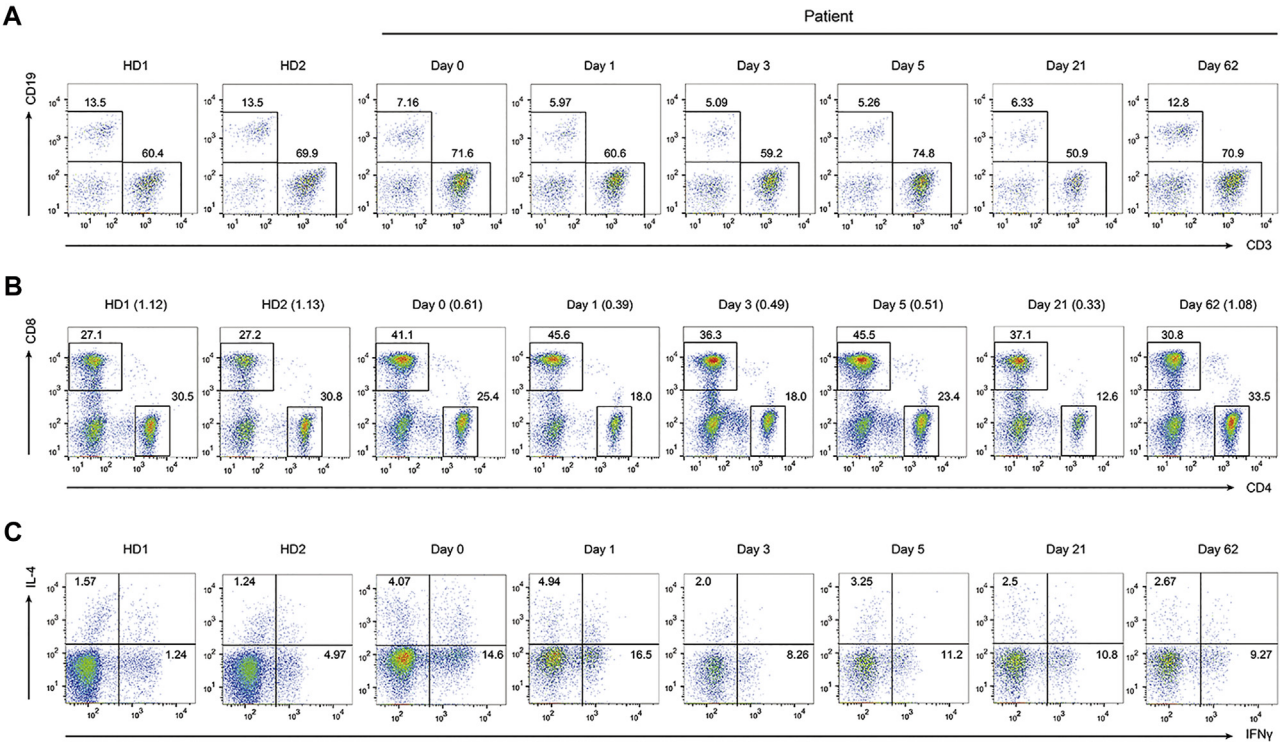

FIG E5. PBMC population analysis. **A,** Lymphocytes were gated on forward scatter/side scatter scattergrams, and $CD19^+$ and $CD3^+$ cells were analyzed. **B,** Lymphocytes were gated on forward scatter/side scatter scattergrams, and $CD4^+$ and $CD8^+$ cells were analyzed. *Numbers in parentheses* indicate ratios of $CD4^+$ cells to $CD8^+$ cells. **C,** Lymphocytes were gated on forward scatter/side scatter scattergrams, and $CD4^+$ cells were gated. After gating, IL-4– and IFN-γ–secreting cells were analyzed. In this analysis isolated cells were stimulated with phorbol 12-myristate 13-acetate (50 ng/mL) and ionomycin (500 ng/mL) in the presence of GolgiPlug (BD PharMingen, San Jose, Calif) for 6 hours.

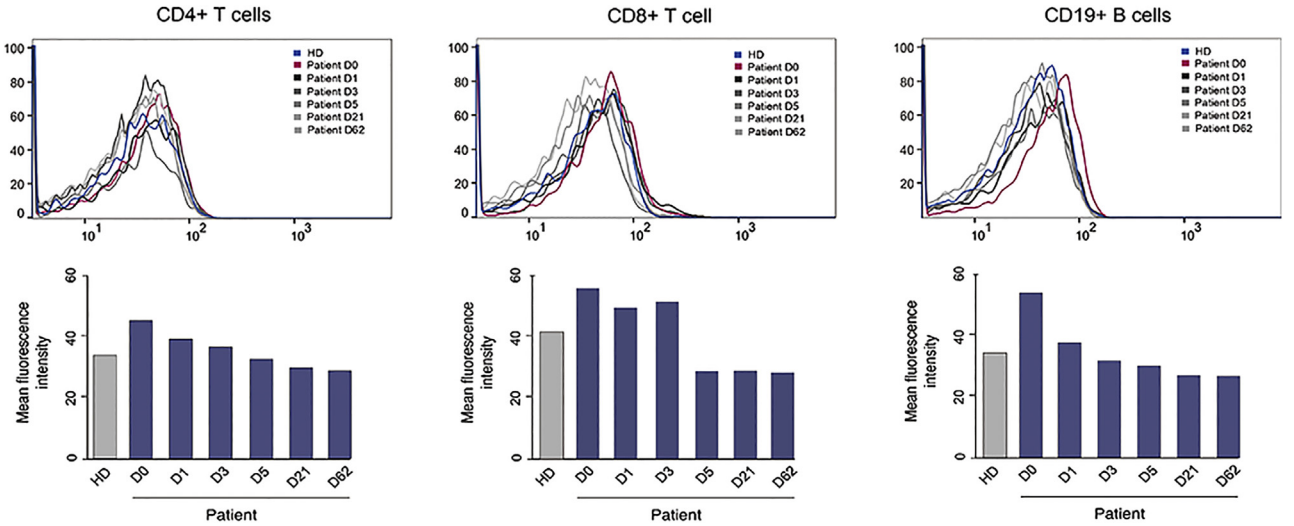

FIG E6. p-STAT levels from $CD4^+$ T cells, $CD8^+$ T cells, and $CD19^+$ B cells after gating lymphocytes based on forward and side scatter.

TABLE E1. Exome run quality summary

Patient	Patient	Mother	Father
Read length (bp)	2 × 74	2 × 74	2 × 74
No. of reads (M)	75.2	65.7	58.8
Median coverage depth (X)	59	51	46
Mean coverage depth (X)	72.5	63.9	57.0
Percentage of reads on genome	91.4	91.5	91.5
Percentage of reads on target	63.2	63.7	63.5
Percentage of bases covered at least 4×	97.9	97.7	97.4
Percentage of bases covered at least 8×	96.4	95.6	94.9
Percentage of bases covered at least 20×	88.4	84.9	82.4
Per-base error rate (%)	0.43	0.42	0.43
Percentage of duplicated reads	4.7	4.7	4.6

TABLE E2. Protein-altering, rare, and patient-specific variants

Type	Gene	Chromosome: position (hg19)	Nucleotide substitution	Zygosity	Effect on protein	Amino acid change	Amino acid location/ protein length	ExAC frequency	SIFT	PolyPhen-2	Coverage (alternative allele/total)		
											Proband	Mom	Dad
De novo	*TMEM173*	5:138860851	A>G	Heterozygous	Missense	p.Ser102Pro	102/379	0	0.22	0.735	13/34	0/33	0/21
De novo	*TMEM173*	5:138857025	A>G	Heterozygous	Missense	p.Phe279Leu	279/397	0	0.12	0.926	24/58	0/47	0/49
De novo	*MYO18A*	17:27419362	G>A	Heterozygous	Missense	p.Ala1729Val	1729/2054	0	0.20	0.242	10/17	0/25	0/28
De novo	*BBS1*	11:66283399	C>T	Heterozygous	Missense	p.Arg196Trp	196/593	2/120,952	0.00	1.000	46/108	0/108	0/103
De novo	*MMP13*	11:102825204	A>T	Heterozygous	Missense	p.Ile165Asn	165/471	0	0.00	0.222	29/68	0/43	0/41
Rare hemizygous	*BRWD3*	X: 79943575	C>T	Hemizygous	Missense	p.Gly1286Glu	1286/1802	0	NA	0.627	77/77	59/131	0/52

TABLE E3. Comparison with previous reports

	Liu et al, 2014[E7]						Jeremiah et al, 2014[E8]				Munoz et al, 2015[E9]	Chia et al, 2016[E10]	Current study
Patient ID	**N1**	**N2**	**N3**	**N4**	**N5**	**N6**	**J1**	**J2**	**J3**	**J4**	**A1**	-	-
Inheritance pattern	Unrelated						Familial				-	-	-
Sex (M/F)	M	F	M	F	F	M	M	M	M	F	M	M	M
Variant origin	*De novo*						NA	Inherited			*De novo*	-	*De novo* (two)
Variant	c.439G>C, p.Val147Leu	c.461A>G, p.Asn154Ser				c.463G>A, p.Val155Met		c.463G>A, p.Val155Met			c.439G>C, p.Val147Leu	c.461A>G, p.Asn154Ser	c.304T>C, p.Ser102Pro & c.835T>C, p.Phe279Leu
Age of onset	Infancy (8 wk)						Adulthood	Teenager	Teenager	Infancy	Infancy	Infancy	Childhood (3 years)
Status at last follow-up	Alive	Alive	Alive	Alive	Dead	Dead	Alive	Dead	Alive	Alive	Alive	Alive	Alive
Rash or Tachypnea	+	+	+	+	+	+	−	+	+	+	+	+	+
Gangrene of finger/toe	4/6						NA				+	+	+
Lung disease	5/6						−	+	+	+	+	+	+
CNS vessel involvement	Not reported						Not reported				Not reported	Not reported	+

F, Female; *M*, male; *NA*, data not available.

TABLE E4. Primers used in this study

Primer name	Primer sequences	Primer name	Primer sequences
TMEM173_S102P_F	5′-AGGAGGATGTTCAGTGCCTG-3′	TMEM173_S102P_R	5′-GGGTATCCAACGTGTGTCAC-3′
TMEM173_F279L_F	5′-ATCAACCCCTCACCCTACCA-3′	TMEM173_F279L_R	5′-GTTACAGGCTGAGGGAGTGG-3′
MYO18A_A1729V_F	5′-CTGTCTAGGGTGAAGGGAGC-3′	MYO18A_A1729V_R	5′-TCTTTCCTGTACAGCCCTCC-3′
BBS1_R196W_F	5′-AGAATGATGGAGGAGGGCAG-3′	BBS1_R196W_R	5′-TGGAAGTCACTGCAGCTTTA-3′
MMP13_I165N_F	5′-CCAGGAGTACTTAGCACAGGT-3′	MMP13_I165N_R	5′-GCCTTCAAAGTTTGGTCCGA-3′
BRWD3_G1286Q_F	5′-TTCTCCAGACTCTGCCTGTG-3′	BRWD3_G1286Q_F	5′-TTGTTCTACTTGCTGCTCCA-3′
IFN-β_qPCR_F	5′-AAACTCATGAGCAGTCTGCA-3′	IFN-β_qPCR_R	5′-AGGAGATCTTCAGTTTCGGAGG-3′